



OPEN

A comprehensive computational study to explore promising natural bioactive compounds targeting glycosyltransferase MurG in *Escherichia coli* for potential drug development

Amneh Shtaiwi¹✉, Shafi Ullah Khan^{2,3}, Meriem Khedraoui⁴, Mohd Alaraj⁵, Abdelouahid Samadi⁶✉ & Samir Chtita⁴

Peptidoglycan is a carbohydrate with a cross-linked structure that protects the cytoplasmic membrane of bacterial cells from damage. The mechanism of peptidoglycan biosynthesis involves the main synthesizing enzyme glycosyltransferase MurG, which is known as a potential target for antibiotic therapy. Many MurG inhibitors have been recognized as MurG targets, but high toxicity and drug-resistant *Escherichia coli* strains remain the most important problems for further development. In addition, the discovery of selective MurG inhibitors has been limited to the synthesis of peptidoglycan-mimicking compounds. The present study employed drug discovery, such as virtual screening using molecular docking, drug likeness ADMET proprieties predictions, and molecular dynamics (MD) simulation, to identify potential natural products (NPs) for *Escherichia coli*. We conducted a screening of 30,926 NPs from the NPASS database. Subsequently, 20 of these compounds successfully passed the potency, pharmacokinetic, ADMET screening assays, and their validation was further confirmed through molecular docking. The best three hits and the standard were chosen for further MD simulations up to 400 ns and energy calculations to investigate the stability of the NPs-MurG complexes. The analyses of MD simulations and total binding energies suggested the higher stability of NPC272174. The potential compounds can be further explored in vivo and in vitro for promising novel antibacterial drug discovery.

Keywords MurG, Natural products, Antibacterial, Antibiotics resistance, Virtual screening, Molecular dynamics, *Escherichia coli*

Diarrhoeagenic *Escherichia coli* (*E. coli*) pathotypes, particularly enteroaggregative *E. coli*, are one of the major food pollutants in gastrointestinal infections worldwide^{1,2}. Causing more than half a million deaths and 1.7 billion morbidities of children under five yearly, thus representing an awful global health issue^{3,4}. Indeed, the existence of *E. coli* has commonly been described in all countries worldwide^{3,5}. And antimicrobial misuse is responsible for a frightening upsurge in bacterial resistance^{6–8}. *E. coli* is a complex group consisting of non-pathogenic and pathogenic strains. When non-pathogenic commensals acquire additional virulence factors, juvenile, adult, pregnant, and immunocompromised individuals sometimes get diseases^{9–11}. In addition, *E. coli* multi-drug

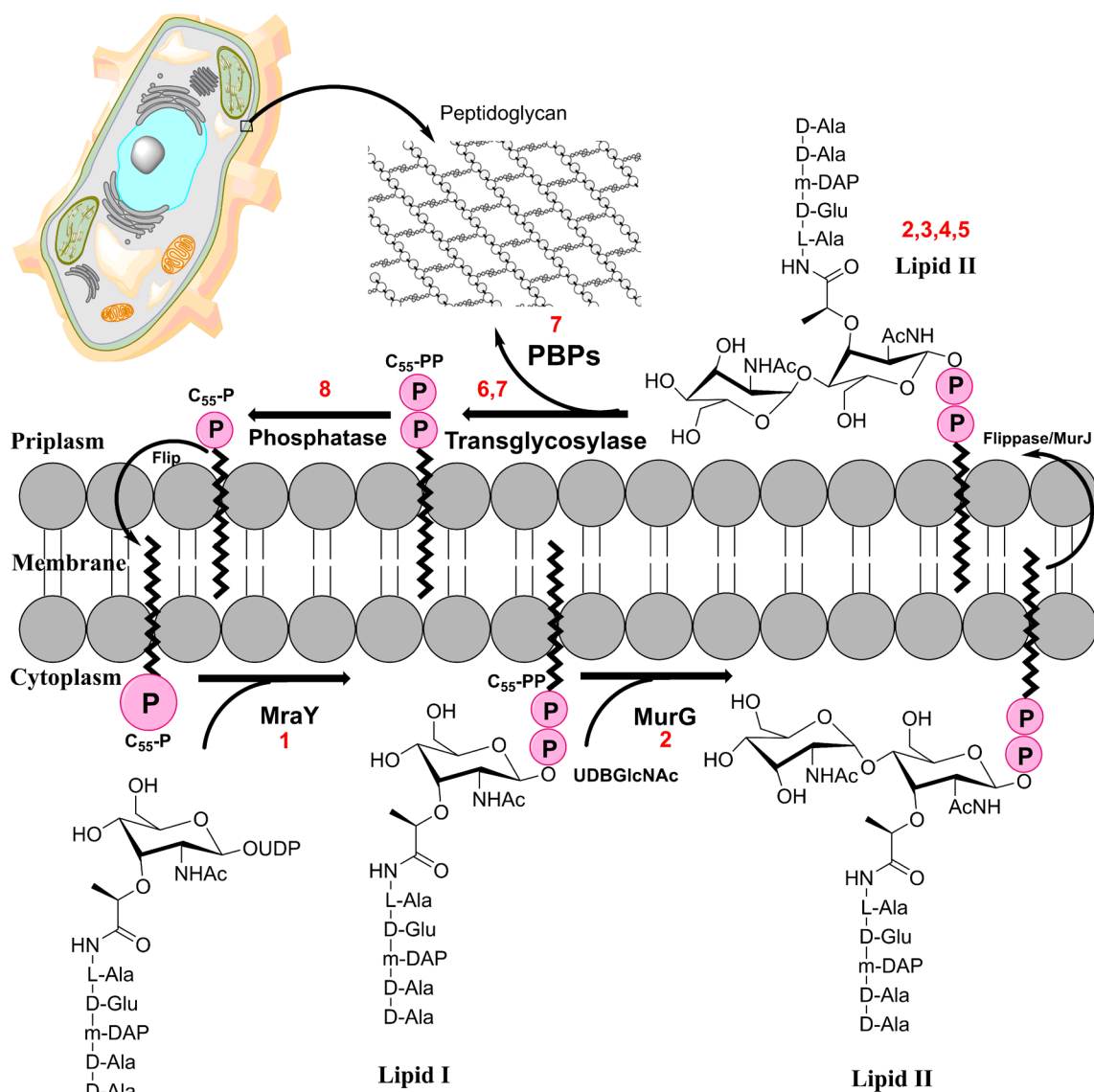
¹Faculty of Pharmacy, Middle East University, Queen Alia Airport Street, Amman, P.O. Box No. 11610, Jordan. ²Interdisciplinary Research Unit for Cancer Prevention and Treatment, Baclesse Cancer Centre, Université de Caen Normandie Inserm Anticipo UMR 1086, Normandie Univ, Research Building, F-14000 François 3 Avenue Général Harris, BP 45026, 14076 Cedex 05 Caen, France. ³Centre François Baclesse, Avenue Général Harris, 14076 Caen Cedex, France. ⁴Laboratory of Analytical and Molecular Chemistry, Faculty of Sciences Ben M'Sik, Hassan II University of Casablanca, B. P 7955, Casablanca, Morocco. ⁵Faculty of Pharmacy, University of Jerash, Jerash, Jordan. ⁶Department of Chemistry, College of Science, UAEU, P.O. Box No. 15551, Al Ain, UAE. ✉email: ashtaiwi@meu.edu.jo; samadi@uaeu.ac.ae

resistance has been detected from numerous sources, likely to increase further with time^{12,13}. Therefore, it is of utmost importance to discover a new lead with potential activity against these resistant bacteria, where the unique potential target could be the MurG glycosyltransferase^{14–18}. This enzyme is crucial for synthesizing the cell wall of *E. coli* bacteria, and thus inhibitors for glycosyltransferases would be effective bactericidal agents^{19–24}.

Peptidoglycan constituents are produced in the cytoplasm and are relocated through the membrane for glycan polymerization via a peptidoglycan constituent synthesis (PCS) cycle that spans the plasma membrane as shown in Fig. 1^{25,26}.

MurG is an enzyme that is essential for the synthesis of peptidoglycan, a structural component of bacterial cell walls. It transfers a GlcNAc molecule from UDP-GlcNAc to lipid I to form lipid II, which is the next step in the synthesis of peptidoglycan^{27,28}. The crystal structures of MurG from *E. coli* and *Pseudomonas aeruginosa* have been resolved, and it has been reported that both are quite similar in structure as shown in Fig. 2^{29–31}. The UDP-GlcNAc molecule is bound tightly to the enzyme in the carboxy-terminal domain, and lipid I interacts with the N-terminal domain³². The enzymes from the two species have different conformations around the hinge domain, but the UDP-GlcNAc scaffold is bound in the same way in both enzymes^{32,33}.

Several agents have been developed to inhibit glycosidase enzymes, but there are only a few uridyl peptide inhibitors available which are summarized in Table 1^{34–42}. These agents are effective against MraY, an enzyme that is essential for bacterial cell wall synthesis. However, some of these agents, such as tunicamycin, are not selective



**1- Uridyl peptides, 2- Ramoplanin, 3- Glycopeptides, 4- Lantibiotics (nisin)
5- Defensin (plectasin), 6- Moenomycin, 7- β -Lactams, 8- Bacitracin**

Figure 1. Peptidoglycan component synthesis (PCS) cycle catalyzed by MraY, MurG and penicillin-binding proteins. Numbers from (1–8) represent common antibiotics targeting the synthesis of bacterial cell walls.

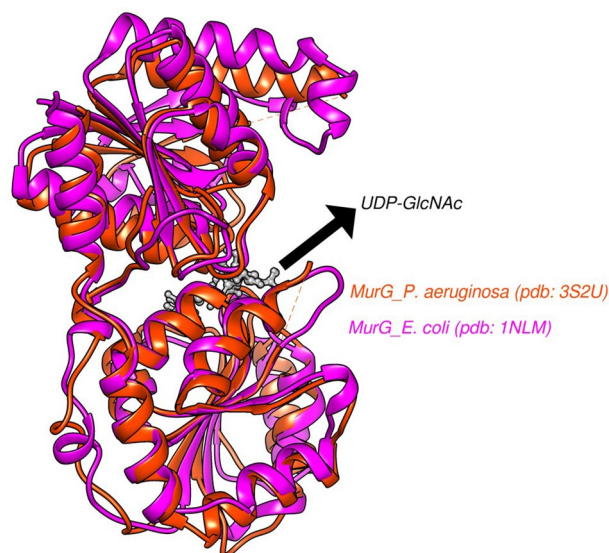


Figure 2. Overlays of the crystal structures of the MurG enzyme from *E. coli* (magenta, PDB code: 1n1m) and *Pseudomonas aeruginosa* (orange, pdb: 3s2u) complexed with UDP-GlcNAc (grey) in the gorge region.

No	Antibiotics	Target	References
1	Uridyl peptides (Mureidomycin A)	MraY	34
2	Ramoplanin	MurG, lipid II	35
3	Glycopeptides	Lipid II	36
4	Lantibiotics (nisin)	Lipid II	37
5	Defensin (plectasin)	Lipid II	38
6	Moenomycin	Transglycosylase	39
7	β -Lactams	PBPs	40,41
8	Bacitracin	Undecaisoprenyl pyrophosphate	42

Table 1. Cell wall biosynthetic antibiotics and their potential targets.

and can also affect human glycol-protein synthesis⁴³. Newer uridyl peptide inhibitors, such as liposidomycins and mureidomycins, are more selective for bacterial glycoprotein biosynthesis. These agents have the potential to be used as new antibiotics for the treatment of bacterial infections^{34,44}.

Many different types of antibiotics such as mannopeptimycins, lantibiotics like ramoplanin, nisin and mercasidin, and defensins like plectasin are also effective by targeting lipid II peptide, an essential component of the bacterial cell wall^{35,37,38}.

Ramoplanin is a lipodepsipeptide that binds to lipid II peptide and inhibits its synthesis. This agent has broad-spectrum activity against methicillin-resistant and vancomycin-resistant gram-positive bacteria⁴⁵. Unlike glycopeptides, ramoplanin does not bind to d-alanine-d-alanine arrangement in the cell wall precursors^{36,46}.

Beta-lactam antibiotics are among the most commonly used antibiotics, and they work by inhibiting the synthesis of cell walls by interacting with penicillin-binding proteins (PBPs)⁴⁷. PBPs are enzymes that are found in both gram-negative and gram-positive bacteria cells and play a role in peptidoglycan transpeptidase and transglycosylase action⁴⁸. There are several mechanisms by which bacteria can develop resistance to beta-lactam antibiotics. The most common mechanism is the production of β -lactamase enzymes, which can break down the beta-lactam ring in the antibiotic molecule, rendering it ineffective⁴⁹. Other mechanisms of resistance include alteration of enzyme PBPs, decreased diffusion of the drug to target PBPs, and efflux pumps^{40,41}. There are a few antibiotics that target other steps in the cell wall synthesis pathway. Moenomycin inhibits the transglycosylase enzyme, but it is not absorbed well and is not clinically useful^{39,50}. Bacitracin inhibits dephosphorylation of C55-isoprenyl pyrophosphate, but it is too toxic for widespread use^{42,51}.

In summary, cell wall drugs are significant antimicrobial agents, and it is important to find new agents for this class to prevent the modification of resistance to these inhibitors. Currently, only a few methods can be used to treat infections caused by highly resistant gram-negative strains. Thus, we aimed to search novel MurG enzyme inhibitors employing a structure based virtual screening method from databases, pursued by ADMET estimation and MD simulations via in silico methods.

Materials and methods

Preparation of the database

The NPASS (Natural Product Activity and Species) database version 1.0 was selected to determine new inhibitors against MurG enzyme^{52,53}. NPASS comprised of 35 thousand natural compounds⁵⁴. All biological compounds were downloaded in SDF file and used for optimization for a new virtual testing process.

Figure 3 illustrates the general method used in this study. We conducted a structure based virtual screening method to choose potential MurG inhibitors from a database consisting of ~30,900 uncommon biological structures utilizing the NPASS version 1.0.38. The NPSS search database was selected because the compounds were extracted from 25 thousand of different natural sources. All data were determined and incorporated with ChEBI, TCMID, UNPD TCM@TaiWan, TCMSP, TM-MCTTD, HerDing, and StreptomeDB. First, biological structures from the NPASS database were saved as SDFs. OMEGA default forcefield mmff94s were then used for conformer construction and energy minimization. Finally, the best compounds with low energy structures were tested through the subsequent virtual testing methods.

NPASS compounds was designed using Discovery Studio, OpenEye, and YASARA software. The 3D optimization of the compounds was performed using Discovery Studio software, followed by energy minimization utilizing YASARA Structure^{55,56}.

Screening and docking studies

The study utilized a molecular docking method for Virtual Screening. Specifically, the bioactive compounds were prepared and subjected to molecular docking employing FRED program version 3.2.0 available in OpenEye software^{57–59}. Prior to docking study, the MurG enzyme was prepared utilizing the pdb2receptor program within OEDocking, and optimization was performed at a neutral pH of 7.0. Subsequently, OMEGA 2.5 was employed to form 200 conformers for each compound through standard settings⁶⁰. The cocrystal ligand was used to define the active site within a 10 Å radius during the docking calculations. Then, the FRED default parameters were employed to calculate the binding energies of the compounds against the MurG enzyme. Ten docked conformations were generated for each ligand using the above-mentioned docking procedure. Finally, the best five hit compounds with the lowest binding energy were selected for molecular simulation study.

E. coli glycosyltransferase (MurG) was determined from the (pdb crystal: 1nlm) of *E. coli* K-12 MurG strain complexed to the UDP_GlcNAc. It has been observed that the UDP_GlcNAc and the natural compounds interact with the MurG catalytic site in a cleavage formed between two domains and consisting of two adjacent pockets: The N-acetylglucosamine ring is accommodated in pocket B, while the uridine forms hydrophobic interactions with pocket A, as depicted in Fig. 4. To validate the procedure, the docking was conducted utilizing the UDP_GlcNAc substrate as a reference. Additionally, for increased result reliability, the size of the docking box was expanded to encompass both the A and B pockets. The FRED docking approach was employed to optimize MurG, aiming to achieve a lower energy level. The crystal structure of UDP_GlcNAc-MurG complex, PDB ID 1nlm, was prepared for docking using Spruce v1.5.2.1 tool in OpenEye Scientific software, with default parameters^{61,62}. Before running Spruce, the homodimer Chain B from protein structure was removed. This was done to isolate the active site of the protein, which is the region where the substrate, UDP_GlcNAc, binds. Spruce effectively splits existing protein–ligand complex and isolates active sites where small molecules are bound to macromolecules. Spruce performs prerequisite preparation of protein structure, including: adding hydrogen atoms to the protein structure to complete its chemical makeup. Optimizing the placement of hydrogen atoms to improve the accuracy of the structure. Expanding the asymmetric unit to its biological counterpart for the X-ray crystallography structures. This ensures that the active site is properly represented in the docked molecule. After completing these tasks, Spruce created a docking-ready receptor. The generated grid box upon the active site had a dimension of 37.884282, –3.588333, and 20.849103 in XYZ dimensions from the obtained design units for the target UDP_GlcNAc-MurG complex⁶³. Following this prerequisite step, validation of docking method was performed by redocking of co-crystallized substrate, UDP_GlcNAc and found to have an RMSD value lower than 2 Å. After though assessment of redocking and validation, all-natural products were subjected to screening. Out of the 30,926 docked natural products, they were sorted based on the binding energies of Fred ChemGuass4, and the best 500 compounds that successfully docked in the MurG binding site were chosen for the next ADMET study.

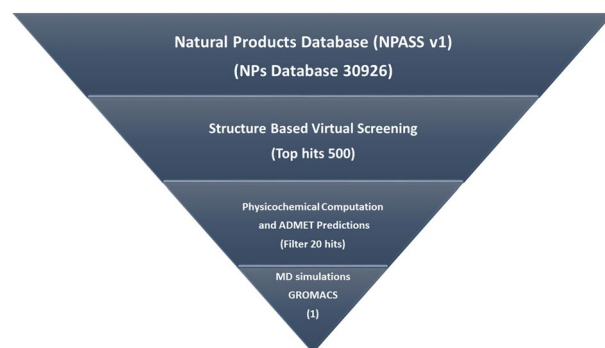


Figure 3. In silico screening method utilized in the study.

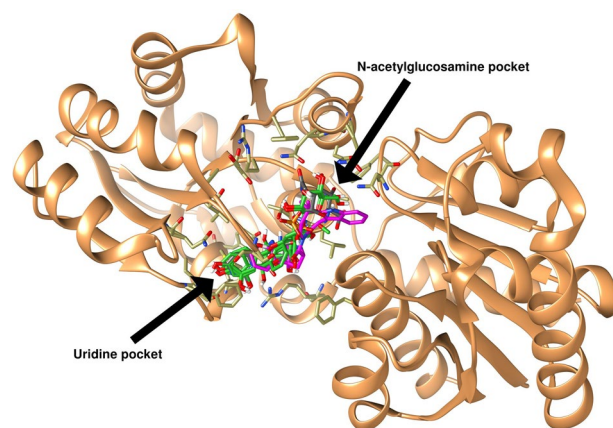


Figure 4. Superimposition of the UDP_GlcNAc native ligand and the top five hits interacted in the MurG active site, pdb:1nlm. Showing the binding poses in a groove between the two domains.

ADMET studies

The SwissADME and admetTSAR2 was employed to calculate the drug-likeness and ADMET properties of the top docked natural product detected from the virtual screening experiment against MurG enzyme^{64,65}.

Molecular dynamics simulation

The dynamic activity of the compound with the lowest two binding energy NPs, NPC727174, NPC170742, and the fifth one NPC259098, in complex with the Glycosyltransferase enzyme MurG (pdb:1nlm), was analyzed through 300 ns simulation. The GROMACS 5.1.4 software program^{66–68} was utilized for conducting the MD simulation, employing the AMBER-FF99SB-ILDN force field⁶⁹. The GROMACS program was employed to generate topology parameters for the MurG receptor, while the small ligands (NPC727174, NPC170742, NPC259098 and the standard UDP_GlcNAc topology parameters were created using ACPYPE from the Amber-Tools package⁷⁰. The systems were placed to periodic cubic box spacing distance of 1.2 nm around the surface and solvated using the TIP3P solvation process at 295 K. To neutralize the systems, counter ions were added to balance the charge of the enzyme. Structural minimization was carried out for 15 thousand steps using the steepest descent protocol under consistent pressure and 295 K, followed by the Berendsen thermostat equilibration run in the NVT (constant number of particles, temperature and volume) ensemble for 200 ps at 300 K. Then, the production runs were performed using the Parrinello–Rahman barostat in the NPT ensemble (constant number of particles, temperature and pressure) for 1 ns at 1 bar and 300 K⁷¹. After the temperature and pressure adjustments, MD simulation runs were performed for the four different systems for 100 ns and a total of 400 ns. VDW and Coulomb interaction cutoffs were adjusted to 12.0 Å and corrected every 2 fs. Moreover, the particle mesh Ewald (PME) protocol was applied to correct ionic contacts⁷². Bond constraints with hydrogen atoms were maintained using LINCS algorithm⁷³. The simulations were conducted with time step of 2.0 femtosecond, and coordinates were recorded at intervals of every 500 step. MD simulation results were analyzed by RMSD, RMSE, structure stability, transition path analysis, and free energy calculations. The visualizations were produced using PyMOL, Discovery Studio and Chimera programs^{55,74,75}.

Free energy calculations

Free energy calculations were performed using the molecular mechanics Poisson–Boltzmann surface area (MM-PBSA) method of the GROMACS software prepared using the gmx_mmpbsa tool⁷⁶. In this study, the last 20 ns of the simulations trajectories of the standard UDP_GlcNAc, and three NPs from the top five structures (NPC727174, NPC170742, and NPC259098) complexes were chosen for energy analysis. MM-PBSA was applied to predict the average binding free energies using a Python script, MmPbSaStat.py. Moreover, the output file summary_energy.dat was obtained and contains the total binding energy of all energetic components (ΔG_{Total}) including the polar solvation energy, ΔE_{PSE} , solvent-accessible surface area (SASA), ΔE_{SASA} , electrostatic interaction, (ΔE_{ele}), and van der Waals interaction, (ΔE_{vdW}). On the other hand, to calculate the average contribution of the residues to the binding energy, the Python script MmPbSaDecomp.py was used, and the results, including the binding energy for each residue, were plotted to show the energy contribution of each significant amino acid residue with its energy. The "Supplementary Python scripts S1 and S2" provide details on the average binding energy calculation and contribution of residues to the binding energy, respectively.

Results and discussion

Binding interactions MurG receptor

The free binding energies of the top 20 MurG-selective natural products were determined and organized based on their ChemGuass4 scores. The FRED binding results were calculated in kcal/mol and presented in (Table 2). In this study, the ChemGuass4 scores exhibit a consistent range for the binding free energies of the 20 NPs to

No	Name	FRED Chemgauss4 score
1	NPC272174	-10.2568
2	NPC170742	-10.0554
3	NPC117260	-9.96509
4	NPC277205	-9.96279
5	NPC259098	-9.81826
6	NPC148409	-9.8013
7	NPC45400	-9.74282
8	NPC245014	-9.62971
9	NPC265454	-9.58556
10	NPC252590	-9.55989
11	NPC307938	-9.53453
12	NPC308931	-9.4984
13	NPC214729	-9.43665
14	NPC124300	-9.41008
15	NPC314573	-9.37501
16	NPC119767	-9.36645
17	NPC263940	-9.26997
18	NPC18185	-9.19354
19	NPC298778	-9.18163
20	NPC154741	-9.12232
Standard	UDP_GlcNAc	-6.29873

Table 2. FRED binding energies of the top twenty natural compounds used in this study.

MurG, falling within -9.70 ± 0.50 kcal/mol, the compound NPC272174 inhibitor (-10.23 kcal/mol) displays best binding affinity, while compound NPC154741 (-9.12 kcal/mol) exhibits the lowest affinity. Later, the potential 5 natural compounds which showed the best ChemGuass4 score are considered for the further studies. The chemical structure, source name and ChemGuass4 score are shown in Table 3. Conversely, Table 4 illustrates the significant binding interactions of the best five compounds with the active site amino acids of MurG enzyme. Additionally, Supplementary (Table S1) provides details on the H-bond donor and acceptor pairs for the best NPs, along with their corresponding lengths.

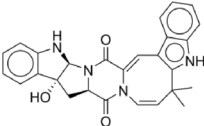
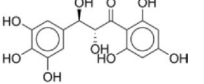
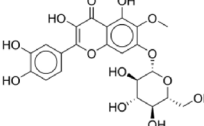
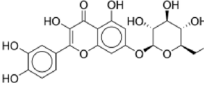
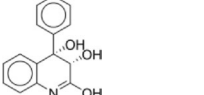
N°	Code	Chemical structure	Common name	Sources	References
1	NPC272174		Okaramine I	Aspergillus aculeatus	82
2	NPC170742		Alpha, Beta, 3,4,5,2',4',6'-Octahydroxydihydrochalcone	Sapium haematospermum	83
3	NPC117260		Patulitrin	Artemisia annua L	84
4	NPC277205		Quercimeritrin	Hyrtilis erecta	85
5	NPC259098		Aflaquinolone F	Aspergillaceae	86

Table 3. Detailed information of the top five natural compounds identified used in this study.

NPs	Interactions	Amino acids
NPC272174	H-Bond	ARG164, SER192, THR266, GLU269
	Pi-Donor H-Bond	ASN128
	Pi-Pi T-shaped	HIS19
	Amide-Pi Stacked	GLY191, SER192
	Pi-Alkyl	ALA264
NPC170742	Hydrogen Bond	ARG164, SER192, THR266, ILE245, SER192, GLU269
	Pi-S	MET248
	Pi-Pi stacked	PHE244
	Pi-Alkyl	LEU265
NPC117260	H-Bond	SER192, ALA264, GLN288, GLU269, GLN289
	Pi-Donor Hydrogen Bond	THR266, THR266
	Pi-S	MET248
	Pi-Pi stacked	PHE244
	Pi-Alkyl	LEU265
NPC277205	H-bond	SER192, ALA264, GLU269, GLN289
	Pi-donor Hydrogen bond	THR266
	Pi-Pi stacked	PHE244, MET248, LEU265
NPC259098	Hydrogen Bond	ARG164, THR266, GLU269
	Pi-Pi Stacked	PHE244
	Pi-Alkyl	ILE245, ILE245, MET248

Table 4. Binding interaction types between the amino acid residues in the MurG active site and the best five natural products.

Drug-likeness and physicochemical analysis

ADMET study, absorption-distribution-metabolism-excretion-toxicity, was employed on the 500 natural products to estimate their Drug-likeness properties. This involved the assessment of their physicochemical properties by evaluating Lipinski, Ghose, Veber, and Egan rule violations^{77,78}. According to ADMET criteria, favorable oral bioavailability is indicated by logP less than five, rotatable bonds less than ten, molecular weight less than 500, and TPSA less than 100, while good intestinal bioavailability is suggested by the number of H-bond donors less than five and acceptors less than ten. The SwissADME tool⁶⁴ was utilized for in-depth analysis of these predictions, and the summarized results are presented in Table 5. Notably, 20 hits from the virtual screening results fell within the acceptable range of drug-like properties based on the Lipinski, Egan, Veber, and Ghose rules. Additionally, the in-silico assessment of these hits based on their physicochemical values indicated favorable pharmacokinetic properties⁷⁹. All parameters are such as Molecular weight = (161–494 g/mol), Flexibility = (0–6) lie within the acceptable range. The number of hydrogen bond acceptors and donors measures the compound's hydrophilicity. A greater value represents increased hydrophilicity, which leads to poor penetration and absorption. On the other hand, the number of hydrogen bond donors less than five and hydrogen bond acceptors less than ten suggests the higher penetration which would improve the absorption. All the compounds except NPC117260 lie within the acceptable number of hydrogen bonds. The (TPSA) Topological Polar Surface Area is used to measure the polar atom's surface area for the compounds. Poorly absorbed compounds and limited cell membrane permeability have been identified as those with a TPSA > 140 Å², while orally rout of administration drugs that undergo transcellular transport should generally not exceed a TPSA of about 140 Å². Therefore, a lower TPSA is considered advantageous for drugs intended for oral administration that undergo transcellular transport⁸⁰. Additionally, a compound with stronger CNS penetration is associated with toxicity and predicted to have a lower TPSA value⁸¹. The studied compounds show values in the range of (53–219) and four of them show high TPSA value greater than 140 Å², NPC298778, NPC277205, NPC170742, and NPC117260 are considered to be poorly absorbed compounds and unable to penetrate the CNS, whereas those with TPSA values less than 140 Å² are considered to increase the membrane permeability.

In the process of drug discovery, a variety of physicochemical properties, collectively known as ADMET properties, play a crucial role in determining the likelihood of a compound entering clinical trials and ultimately becoming a successful drug. These properties encompass Molecular Weight (MW), which assesses a compound's size and its ability to cross biological membranes; Number of Rotatable Bonds (nRot), which evaluates a compound's flexibility and its susceptibility to unwanted transformations in the body; Number of Hydrogen Bond Acceptors (nHBacc), which gauges a compound's capacity to interact with and bind to proteins; Number of Hydrogen Bond Donors (nHBDdon), which predicts a compound's potential to be metabolized by enzymes; and Topological Polar Surface Area (TPSA), which measures a compound's overall polarity and its ability to interface with water and other polar molecules. Generally, compounds with values within the following acceptable criteria are considered to have a higher likelihood of proving successful drug candidates: MW < 500 g/mol, nRot < 10, nHBacc < 10, nHBDdon < 5, TPSA < 140 Å². These criteria serve as valuable guidelines for early-stage

Compound	Molecular weight	Rotatable bonds	H-bond acceptors	H-bond donors	TPSA	Violations			
						Lipinski	Ghose	Veber	Egan
NPC105415	382.45	5	5	3	86.99	0	0	0	0
NPC117260	494.40	5	13	5	219.74	1	1	1	1
NPC119767	390.34	4	7	3	121.13	0	0	0	0
NPC124300	400.38	4	9	3	131.23	0	0	0	0
NPC148409	271.22	0	6	3	92.04	0	0	0	0
NPC170742	338.27	4	9	8	178.91	1	0	1	1
NPC214729	328.32	4	6	3	96.22	0	0	0	0
NPC223136	302.32	5	5	3	79.15	0	0	0	0
NPC252590	161.16	0	3	2	53.35	0	1	0	0
NPC259098	255.27	1	4	3	73.05	0	0	0	0
NPC265454	330.37	8	5	4	97.99	0	0	0	0
NPC272174	452.50	0	3	3	88.67	0	1	0	0
NPC276930	260.20	0	6	4	111.13	0	0	0	0
NPC277205	464.38	4	10	4	210.51	1	1	1	1
NPC298778	486.47	6	10	3	148.82	0	1	1	1
NPC308931	328.37	2	2	3	73.04	0	0	0	0
NPC314573	348.44	5	4	2	66.24	0	0	0	0
NPC329077	246.22	2	7	4	122.82	0	1	0	0
NPC44530	302.28	0	6	5	110.38	0	0	0	0
NPC470802	426.50	6	6	5	110.38	0	0	0	0

Table 5. Drug likeness analysis and physicochemical results of the best 20 natural products.

drug discovery efforts, helping researchers identify compounds with favorable physicochemical properties that are more likely to progress through the drug development pipeline and ultimately reach patients.

Detailed ADMET analysis of top20 compounds are shown in Table 6. NPC105415 exhibits generally favourable ADME properties, with several desirable characteristics and minimal potential for adverse effects. It is not predicted to cause skin irritation or sensitization, and it exhibits a low likelihood of carcinogenicity and CYP enzyme inhibition. Additionally, its biodegradability and human intestinal absorption are both favorable. However, despite its overall positive profile, NPC105415 raises some concerns regarding its Ames mutagenicity, nephrotoxicity, reproductive toxicity, and plasma protein binding. These properties warrant further investigation to assess their potential impact on human health. NPC105415 exhibits a blend of favorable and potentially concerning ADME properties. While its low acute oral toxicity, low water solubility, and moderate plasma protein binding suggest a low likelihood of adverse effects, its Ames mutagenicity, nephrotoxicity, reproductive toxicity, and respiratory toxicity warrant further investigation. Additional studies are required to fully characterize NPC105415's ADME profile and assess its potential impact on human health. Contrary to the compound with the highest binding affinity in terms of molecular docking and MD simulation, further in-depth analysis of the ADME assessment of other compounds revealed that the other top compounds NPC117260 and NPC148409 possessed favorable properties in terms of Ames mutagenicity, nephrotoxicity, reproductive toxicity, and plasma protein binding. These findings suggest that the compound at the top of the list may have superior activity but may face challenges in advancing to the next phase due to ADME concerns, requiring optimization to enhance ADME properties.

The analysis of the binding modes for the top five natural compounds interacting with the MurG binding site was conducted to uncover their interactions. Notably, ARG164, SER192, THR266, and GLU269 emerged as crucial key residues involved in hydrogen bond interactions. Conversely, PHE244, LEU265 and MET248 amino acid residues are essential for hydrophobic interactions, namely pi-alkyl and pi-pi stacked interactions for all ligands except the top hit NPC272174, which involved in the hydrophobic interactions with surrounding amino acid residues HIS19, GLY191, SER192 and ALA264. Moreover, NPC170742 and NPC117260 ligands forms pi-sulfur interaction between MET248 and the aromatic ring of the ligand as shown in Fig. 5.

It's noteworthy that among all the binding site residues, Gln289, Gln288, ARG164, and GLU269 of *E. coli* MurG play a significant role in the interaction with UDP_GlcNAc substrate^{46,87}. Additionally, observations indicate that the MurG active site features a conserved pocket as shown in Fig. 5F^{29,30}. This implies that the frameworks of the top five NPs form similar binding interactions as the UDP_GlcNAc substrate, as illustrated in Fig. 5. Comparing the interacting residues involved in binding interaction for the top five compounds, we observe some similarities and differences. Both NPC272174 and NPC170742 interact with ARG164, SER192, THR266, and GLU269 via hydrogen bonds, but NPC170742 also has additional interactions with ILE245 and a pi-sulfur bond with MET248. In contrast, NPC272174 has a pi-donor H-bond with ASN128 and π - π T-shaped interaction with HIS19. Both NPC117260 and NPC277205 interact with SER192, ALA264, GLU269, and THR266 (via pi-donor hydrogen bonds), as well as PHE244 via π - π stacked interactions, but NPC117260 also interacts with GLN288 and GLN289 via hydrogen bonds and MET248 via a π -sulfur bond. NPC277205 has an additional π - π

	NPCI05415	NPCI17260	NPCI19767	NPCI24300	NPCI48409	NPCI70742	NPC214729	NPC223136	NPC252590	NPC259098	NPC265454	NPC272174	NPC276930	NPC277205	NPC298778	NPC308931	NPC314573	NPC329077	NPC44530	NPC470802
Skin corrosion	-	-	-	-	-	-	-	-	-	-	-	-	-	-	-	-	-	-	-	-
Skin irritation	+	-	-	-	-	-	-	-	-	-	-	-	-	-	-	-	-	-	-	-
Skin sensitisation	+	-	-	-	-	-	-	-	-	-	-	-	-	-	-	-	-	-	-	-
Human oral bioavailability	-	-	-	-	-	-	-	-	+	-	-	-	-	-	-	-	-	-	-	-
Blood Brain Barrier	+	-	-	-	-	-	-	-	+	-	-	+	-	-	-	-	-	-	-	-
Biodegradation	-	-	-	-	-	-	-	-	-	-	-	-	-	-	-	-	-	-	-	-
Carcinogenicity (binary)	-	-	-	-	-	-	-	-	-	-	-	-	-	-	-	-	-	-	-	-
CYP1A2 inhibition	-	+	-	-	+	-	-	-	-	+	-	+	-	-	+	-	-	-	+	-
CYP2C9 inhibition	-	-	-	-	-	-	-	-	-	-	-	-	-	-	-	-	-	-	-	-
CYP2D6 inhibition	-	-	-	-	-	-	-	-	-	-	-	-	-	-	-	-	-	-	-	-
CYP inhibitory promiscuity	-	-	-	-	-	-	-	-	-	-	-	+	-	-	+	-	-	-	-	-
Hepatotoxicity	+	-	-	-	+	-	-	-	-	+	-	+	-	-	+	-	-	-	-	+
Human Intestinal Absorption	+	-	-	-	+	-	-	-	+	-	-	+	+	-	+	-	+	+	+	+
Ames mutagenesis	+	-	+	+	-	-	-	+	-	+	+	-	-	+	+	-	+	+	+	+
Nephrotoxicity	+	-	-	-	+	-	-	-	-	+	-	+	-	+	+	-	-	-	-	-
Reproductive toxicity	+	-	+	+	+	+	+	+	+	+	+	+	+	+	+	-	+	+	+	+
Acute Oral Toxicity	2.72	2.92	2.44	2.31	2.73	2.46	1.97	2.26	2.00	1.52	1.98	1.93	1.79	1.78	2.37	2.13	3.05	3.05	2.30	2.50
Plasma protein binding	1.06	0.78	0.75	0.79	0.88	1.08	0.55	0.73	0.59	1.01	0.73	0.91	0.75	0.65	0.92	1.11	1.07	1.07	0.93	0.94
Water solubility (logS)	-3.17	-1.96	-2.32	-2.45	-3.35	-2.95	-2.45	-2.45	-2.62	-2.71	-2.45	-2.71	-2.90	-3.16	-4.24	-3.18	-3.26	-3.26	-3.96	-2.66

Table 6. Comprehensive Assessment of ADME properties and toxicities of the best 20 natural products used in this study.

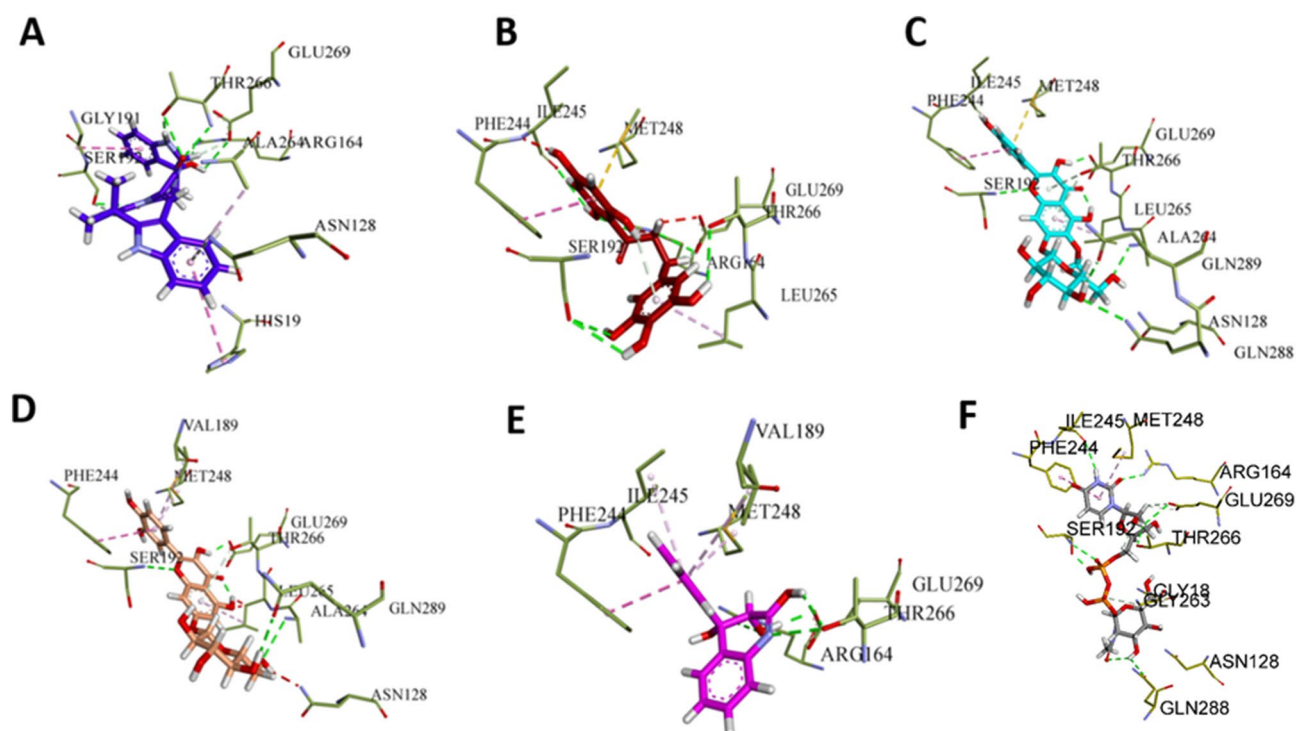


Figure 5. Docking structures of the best five NPs interacted with MurG binding site of *E. coli*. Ligands are presented in stick, while MurG residues are depicted in thin-stick with olive colour. The structures of A, B, C, D, E and F are NPC272174, NPC170742, NPC117260, NPC277205, NPC259098 NPs and UDP_GlcNac, respectively. Important hydrogen bonds are highlighted.

stacked interaction with MET248 and π -alkyl interactions with LEU265. NPC259098 interacts with ARG164, THR266, and GLU269 via hydrogen bonds, and PHE244 via π - π stacked interactions, as well as π -alkyl contacts with ILE245 and MET248.

Although the binding scores for the top five compounds are relatively close, ranging from -10.257 to -9.818 , the differences in their specific interactions with amino acid residues may account for differences in their overall binding and biological activities. The various types of interactions play significant roles in ligand-protein binding, contributing to the specificity and strength of the interaction. Hydrogen bonds, which are relatively common, help stabilize the complex and contribute to the specificity of the interaction. π - π stacking contributes to the strength of the interaction and helps to orient the ligand in the binding site. π -alkyl interactions help increase the affinity of the ligand for the protein by reducing the overall energy of the complex. π -donor hydrogen bonds contribute to the specificity of the interaction and stabilize the complex, while π -sulfur interactions aid to orient the NPs in the binding site and contribute to the strength of the interaction.

MD simulation analysis

Promising natural products (NPC272174, NPC170742, and NPC259098) and the standard UDP_GlcNac stabilities within the active site of the MurG receptor were evaluated through a 100 ns MD simulation for each until the system reached convergence. The resulting total 400 ns trajectory was analyzed using root mean squared deviation (RMSD) to evaluate the dynamic behavior and stabilities of the standard and NPs-1nM complexes, radius of gyration (Rg), root mean square fluctuation (RMSF), transition path analysis, and free energy calculations. The “Supplementary video S1” provides details on the 100 ns MD simulations of the best-hit NPC272174 during the complexation with the MurG enzyme in *Escherichia coli*.

Root means squared deviation

Following the MD simulation, structural changes and stability were assessed by studying the root mean squared deviation from the start of the simulation runs and the initial conformational structures. RMSD calculates the deviation in the complex conformation compared to its initial conformation, providing insight into any changes in the structures during the complexation of ligands-MurG systems. Figure 6 illustrates the RMSD curve during the time for the (NPC272174, NPC170742, NPC259098, and standard UDP_GlcNac) with MurG complexes. Throughout the experiment, it can be observed that the NPC272174-MurG complex undergoes a relative increase in RMSD values from the start of simulation to 0.35 nm within the first 10 ns as shown in Fig. 6a as compared to the standard UDP_GlcNac. The high RMSD fluctuation from 0 to 30 ns appears to have happened due to the conformational change of the NPC272174 compound inside the MurG active site. Then, the plot began to stabilize after 30–100 ns. This result indicates that NPC272174 encourages the stability of the NPC272174-MurG complex. In addition, the NPC170742 complex behaves with the same increased fluctuation at the first

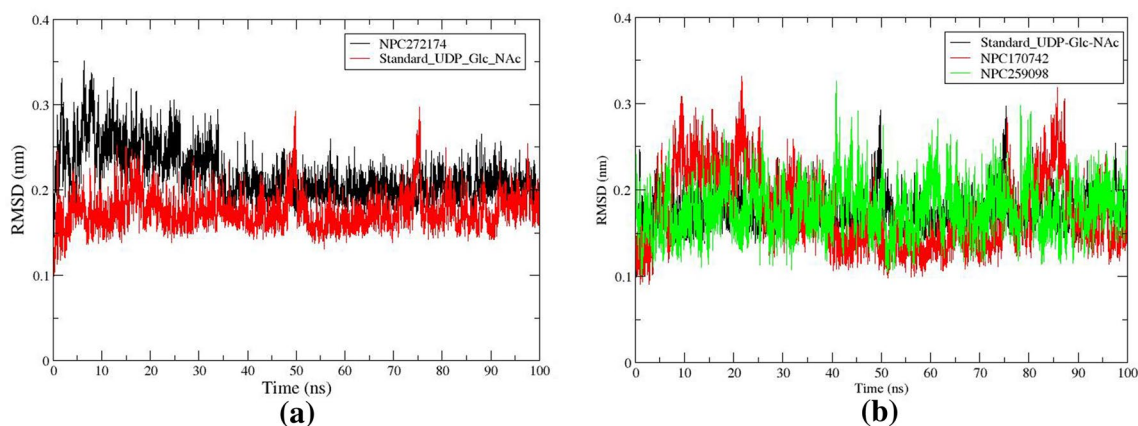


Figure 6. RMSD curve of the complexes of (a) NPC272174 and standard UDP_GlcNAc. (b) NPC170742, NPC259098, and standard UDP_GlcNAc backbone atoms complexed with MurG enzyme of *E. coli*.

30 ns, Fig. 6b, while the NPC259098 complex behaves with constant fluctuations with an RMSD value of 0.2 nm. However, the overall RMSD for the NP complexes was consistently lower over the simulation time, indicative of the fact that the complexes after 30 ns simulation time remained largely unchanged from the original input structure and were reasonably stable and capable of maintaining its conformation, specifically the best-hit NPC727174-MurG complex structure.

Radius of gyration

The radius of gyration (R_g) serves as an indicator of the folding stability of the MurG receptor during the interaction of NP compounds. High folded enzyme conformation is reflected in greater compactness, resulting in a lower R_g value. Conversely, an increasing R_g value suggests less compactness and indicates an unfolded structure. In the present study, R_g was employed to assess the compactness of the systems throughout the simulations, and the R_g plots are shown in Fig. 7. The findings reveal R_g scores ranging between 2.15 and 2.25 nm for NPC727174-MurG complex, Fig. 7a. The reported R_g value for the MD simulation was 2.17 nm over the simulation time. While minor flexibility was observed at the beginning of the MD simulation, the values quickly became constant and fluctuated within a permitted range after 30 ns. NPC170742 and NPC259098 complexes behaved as NPC727174 complex with R_g scores ranging between 2.12 and 2.24 nm as shown in Fig. 7b.

Root mean squared fluctuations

To describe the fluctuations and structural changes within the NP-MurG complexes, root mean square fluctuations (RMSF) were studied and the results are depicted in Fig. 8. Investigation of the RMSFs indicates that the most elevated fluctuation, approximately 0.30 nm, occurred consistently throughout the simulation period for NPC727174 and the standard UDP_GlcNAc. This high fluctuation was associated with amino acid residues ALA76, Ile75, ALA77, Arg180, and GLU181, Fig. 8a, which were observed in the N-terminal region and the loop in the carboxy-terminal side as shown in Fig. 8c. In addition, it has been observed that the NPs NPC170742 and NPC259098 have the same fluctuation regions in the MurG enzyme. This observation agrees with a prior

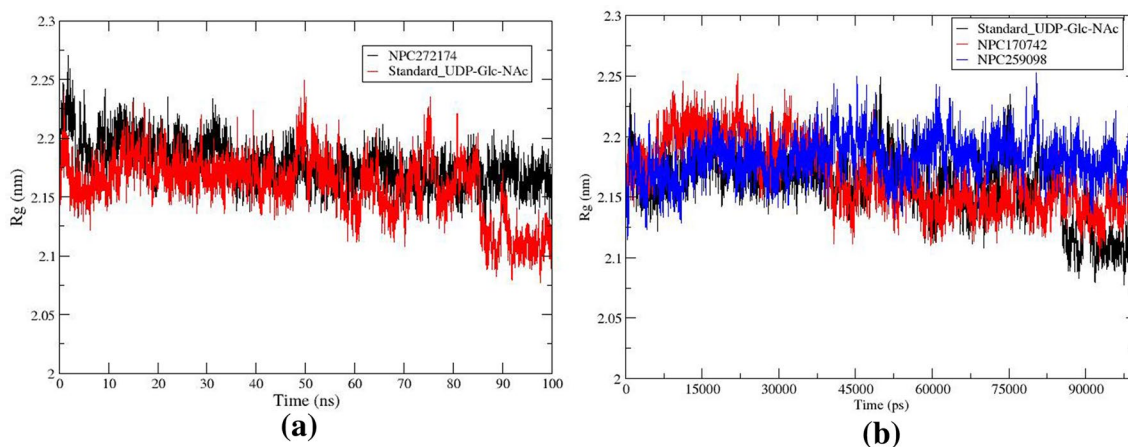


Figure 7. R_g profile of the compounds (a) NPC272174 and standard UDP_GlcNAc. (b) NPC170742, NPC259098, and standard UDP_GlcNAc complexed with MurG enzyme of *E. coli*.

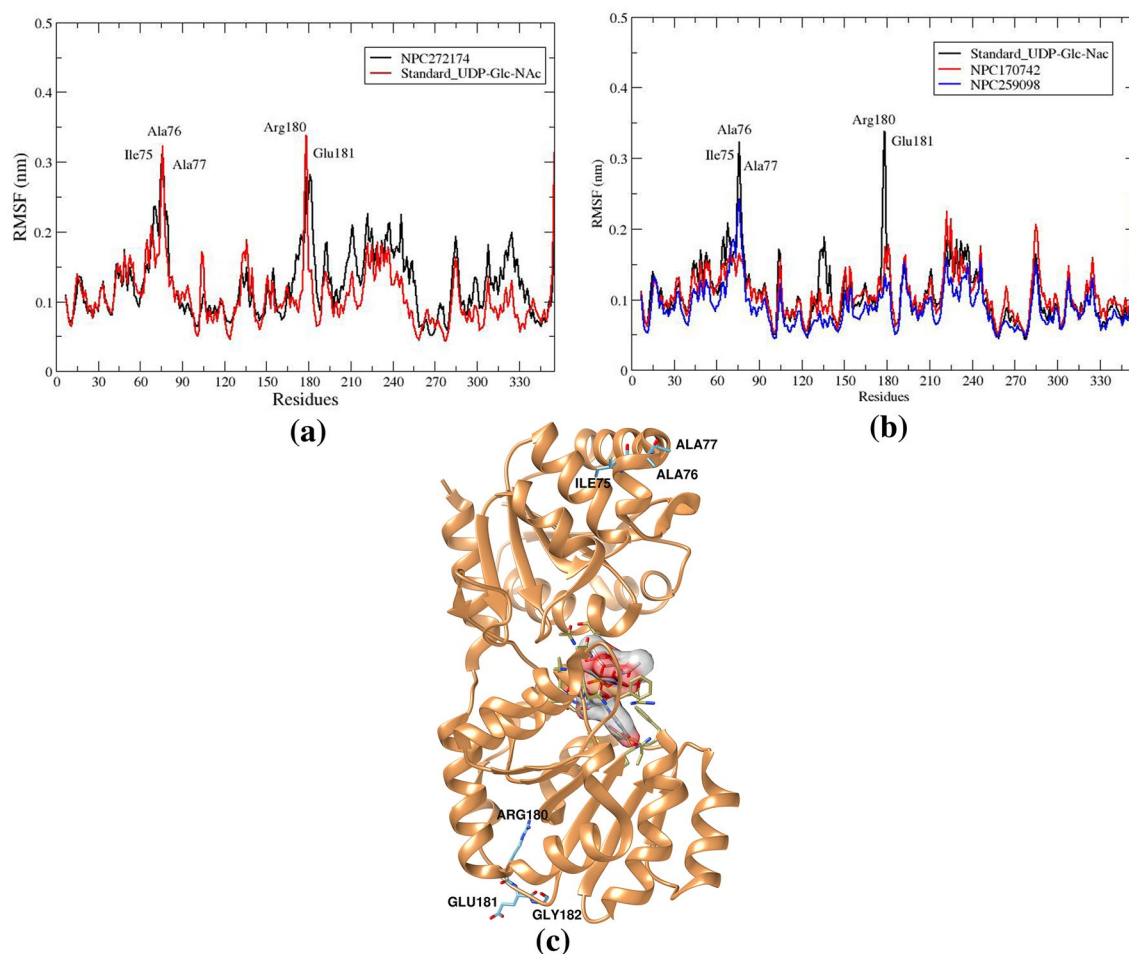


Figure 8. Fluctuation profile (a) RMSF plot of the NPC272174 and standard UDP_GlcNac compounds. (b) RMSF plot of the NPC170742, NPC259098, and standard UDP_GlcNac compounds complexed with MurG enzyme during the simulation time. (c) Amino acid residues involve the highest RMSF value in the ligands-MurG complex structures.

study including the crystal of MurG, which identified flexible areas in the carboxy-terminal and N-terminal amino acid residues^{31,87}.

Free energy analysis

The MM-PBSA method has been applied to predict binding free energy and to evaluate the relative stability of the NPC727174, NPC170742, NPC259098, and the standard UDP_GlcNac complexed with the MurG enzyme. The calculated total binding energy for MD trajectories and the obtained binding free energy components are shown in Table 7. As can be seen, the calculated free energies, ΔG_{Total} , of MurG enzyme towards the different NPs and the standard are in the order of NPC259098, $-15.64 \text{ kJ mol}^{-1}$ > NPC170742, $-20.72 \text{ kJ mol}^{-1}$ > NPC727174, $-33.64 \text{ kJ mol}^{-1}$ > UDP_GlcNac, $-40.57 \text{ kJ mol}^{-1}$.

From the contribution of the calculated energy components of the binding free energies in the NPC727174, NPC259098, and the standard UDP_GlcNac as shown in Table 7, the main driving force for the binding

Energy components	NPC727174	NPC170742	NPC259098	UDP_GlcNac
van der Waals (ΔE_{vdw})	-21.31	-21.98	-26.19	-51.68
Electrostatic (ΔE_{ele})	-60.88	-67.51	-7.8	-71.39
Polar solvation (ΔE_{pse})	56.40	72.78	21.37	89.77
SASA (ΔE_{SASA})	-3.88	-4.01	-3.01	-7.27
Total binding energy (ΔG_{Total})	-33.64	-20.72	-15.64	-40.57

Table 7. Calculated binding free energies (in kJ mol^{-1}) and their components based on the MM-GBSA method for the three MurG-NPs complexes and the standard UDP_GlcNac-MurG complex.

interactions is electrostatic and van der Waals interactions. The polar solvation contributed unfavourably to the binding of the ligand to MurG enzyme. Indeed, the electrostatic, van der Waals non polar, and SASA interactions contribute favourably towards the binding of all ligands to MurG enzyme and are compensated by the large polar solvation energy.

A detailed analysis of the binding energy contributions was analysed using the MM-PBSA method. Figure 9 shows the energy contributions in kcal mol⁻¹ of the ligand–receptor per-residue interaction for the standard UDP_GlcNAc and NPC727174 ligand systems. During the simulation of the standard UDP_GlcNAc complex, the energy appears mainly from the binding with the polar Glu269 amino acid residue and nonpolar Phe244, Ile245 and Met248 amino acid residues, Fig. 9a. On the other hand, the nonpolar amino acid residue of the NPC727174 complex interactions mainly arose from Phe21, Phe244 and Met248 Leu265, with the strongest interactions from Leu265 amino acid residue as shown in Fig. 9b. In addition, amino acid residues Glu269 made obvious polar contributions to NPC727174 with lowest binding energy value and strongest interaction as compared to the standard UDP_GlcNAc complex. This indicates that the polar amino acid residue interaction stabilizes the NPC727174–MurG interaction during the simulation. While the stability of the UDP_GlcNAc ligand in the MurG active site is achieved via hydrophobic and polar interactions.

Analysis of the complex transition path

The motions of NPC272174 and MurG enzyme complex at different simulation periods were investigated and shown in Fig. 10. The most changes involve the coil of the C-terminal and hinge regions which move fast at the start of the simulation time, and this agrees with the increased fluctuation results obtained from the RMSD plot at the first 30 ns, then persistent value was observed for the remaining simulation time till 100 ns. The transition path results indicate that NPC272174 natural compound enhances the complex stability along the simulation time.

Conclusion

Many studies identified inhibitors for the antibiotic target MurG enzyme. However, the nucleus structure for large MurG enzyme inhibitors is restricted to peptidoglycan-mimicking scaffolds, thus simulating the resistance of drugs in the *E. coli* strains. Consequently, the development of new MurG potential inhibitors has increased to a favorable approach. We analyzed the best five hits from the NPASS database of natural products as potential MurG inhibitors, followed by the drug-likeness assessment using a computational prediction method. The results indicated that the promising NPs bind with an increased affinity, mimicking the binding of the UDP_GlcNAc substrate. The best five hits form H-bond interaction with important amino acid residues of ARG164, SER192,

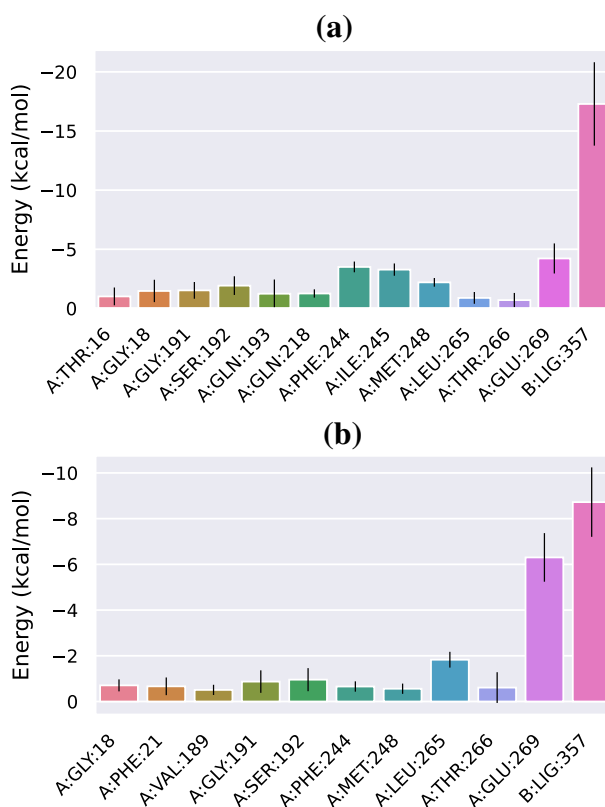


Figure 9. Energetic components per-residue decomposition of (a) the standard UDP_GlcNAc. (b) NPC727174 complexes with MurG enzyme of *E. coli*.

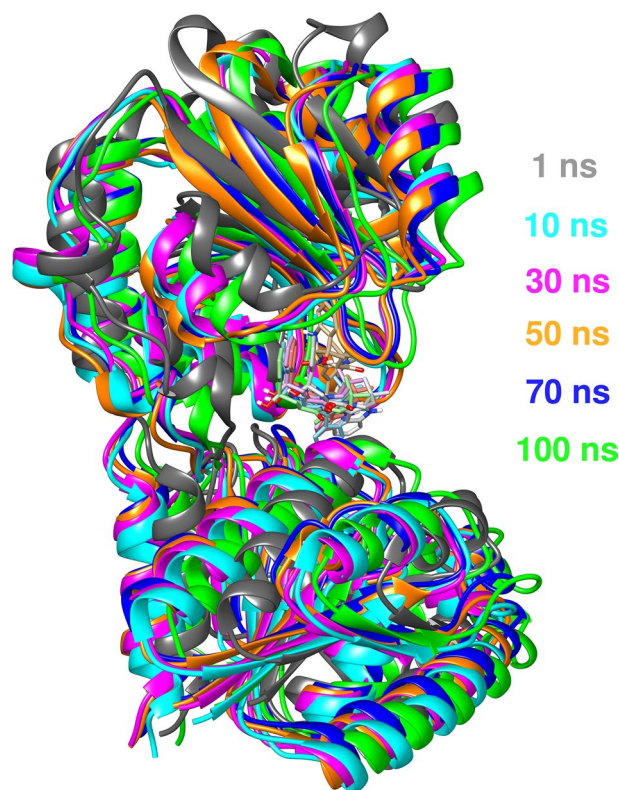


Figure 10. Overlays of the conformational dynamics snapshot for NPC272174-MurG complex taken at different simulation times. The conformation colors corresponding to the appropriate time are highlighted.

THR266, and GLU269. A molecular dynamics simulation study of the best three candidate natural compounds complexed with MurG demonstrated strong stability of NPC272174 to the enzyme structure. In addition, upon comparing the MM-PBSA binding free energy values for the three NPs, the results suggest that the complexation of NPC272174 to the MurG is more favorable. Therefore, the identified NPs suggest that the potential NPC272174 compound is a promising novel scaffold inhibitor for the MurG protein in *E. coli* as an antibacterial agent.

Data availability

All data generated or analysed during this study are included in this published article [and its supplementary information files].

Received: 24 November 2023; Accepted: 21 March 2024

Published online: 26 March 2024

References

- Bélangier, L. *et al.* *Escherichia coli* from animal reservoirs as a potential source of human extraintestinal pathogenic *E. coli*. *FEMS Immunol. Med. Microbiol.* **62**, 1–10. <https://doi.org/10.1111/j.1574-695X.2011.00797.x> (2011).
- World Health Organization. WHO estimates of the global burden of foodborne diseases: foodborne disease burden epidemiology reference group 2007–2015. World Health Organization. <https://apps.who.int/iris/handle/10665/199350> (2015)
- Bhusal, B. *et al.* Multi-drug resistance, β -lactamases production, and coexistence of bla (NDM-1) and mcr-1 in *Escherichia coli* clinical isolates from a referral hospital in Kathmandu. *Nepal. Microbiol. Insights* **16**, 1–8. <https://doi.org/10.1177/11786361231152220> (2023).
- World Health Organization Diarrhoeal Disease. World Health Organization. <https://www.who.int/news-room/fact-sheets/detail/diarrhoeal-disease> (2017)
- Kotloff, K. L. *et al.* The incidence, aetiology, and adverse clinical consequences of less severe diarrhoeal episodes among infants and children residing in low-income and middle-income countries: a 12-month case-control study as a follow-on to the Global Enteric Multicenter Study (GEMS). *Lancet* **7**, e568–e584. [https://doi.org/10.1016/s2214-109x\(19\)30076-2](https://doi.org/10.1016/s2214-109x(19)30076-2) (2019).
- Boucher, H. W. *et al.* Bad bugs, no drugs: no ESKAPE! An update from the infectious diseases society of America. *Clin. Infect. Dis.* **48**, 1–12. <https://doi.org/10.1086/595011> (2009).
- Terajima, J., Izumiya, H., Hara-Kudo, Y. & Ohnishi, M. Shiga toxin (verotoxin)-producing *Escherichia coli* and foodborne disease: A review. *Food Saf.* **5**, 35–53. <https://doi.org/10.14252/foodsafetyfscj.2016029> (2017).
- French, G. L. The continuing crisis in antibiotic resistance. *Int. J. Antimicrob. Agents.* **36**(Suppl 3), S3-7. [https://doi.org/10.1016/s0924-8579\(10\)70003-0](https://doi.org/10.1016/s0924-8579(10)70003-0) (2010).
- Chaudhuri, R. R. & Henderson, I. R. The evolution of the *Escherichia coli* phylogeny. *Infect. Genet. Evol.* **12**, 214–226. <https://doi.org/10.1016/j.meegid.2012.01.005> (2012).
- Byrne, L. *et al.* Epidemiology and microbiology of Shiga toxin-producing *Escherichia coli* other than serogroup O157 in England, 2009–2013. *J. Med. Microbiol.* **63**, 1181–1188. <https://doi.org/10.1099/jmm.0.075895-0> (2014).

11. De Oliveira, A. C., Damasceno, Q. S., Piscocya, M. & Nicoli, J. R. Epidemiologic characteristics of resistant microorganisms present in reserves from an intensive care unit. *Am. J. Infect. Control.* **40**, 186–187. <https://doi.org/10.1016/j.ajic.2011.04.010> (2012).
12. Ibrahim, M. E., Bilal, N. E. & Hamid, M. E. Increased multi-drug resistant *Escherichia coli* from hospitals in Khartoum state. *Sudan. Afr. Health Sci.* **12**, 368–375. <https://doi.org/10.4314/ahs.v12i3.19> (2012).
13. Raju, B. & Ballal, M. Multidrug resistant enteroaggregative *Escherichia coli* diarrhoea in rural southern Indian population. *Scand. J. Infect. Dis.* **41**, 105–108. <https://doi.org/10.1080/00365540802641856> (2009).
14. Mann, P. A. *et al.* Murgocil is a highly bioactive staphylococcal-specific inhibitor of the peptidoglycan glycosyltransferase enzyme MurG. *ACS Chem. Biol.* **8**, 2442–2451. <https://doi.org/10.1021/cb400487f> (2013).
15. Helm, J. S., Chen, L. & Walker, S. Rethinking ramoplanin: The role of substrate binding in inhibition of peptidoglycan biosynthesis. *J. Am. Chem. Soc.* **124**, 13970–13971. <https://doi.org/10.1021/ja021097n> (2002).
16. Trunkfield, A. E., Gurcha, S. S., Besra, G. S. & Bugg, T. D. H. Inhibition of *Escherichia coli* glycosyltransferase MurG and Mycobacterium tuberculosis Gal transferase by uridine-linked transition state mimics. *Bioorg. Med. Chem.* **18**, 2651–2663. <https://doi.org/10.1016/j.bmc.2010.02.026> (2010).
17. Saxena, S., Abdullah, M., Sriram, D. & Guruprasad, L. Discovery of novel inhibitors of Mycobacterium tuberculosis MurG: Homology modelling, structure based pharmacophore, molecular docking, and molecular dynamics simulations. *J. Biomol. Struct. Dyn.* **36**, 3184–3198. <https://doi.org/10.1080/07391102.2017.1384398> (2018).
18. Helm, J. S., Hu, Y., Chen, L., Gross, B. & Walker, S. Identification of active-site inhibitors of MurG using a generalizable, high-throughput glycosyltransferase screen. *J. Am. Chem. Soc.* **125**, 11168–11169. <https://doi.org/10.1021/ja036494s> (2003).
19. Amara, G. M. *et al.* Screening of promising molecules against MurG as drug target in multi-drug-resistant *Acinetobacter baumannii*: Insights from comparative protein modeling, molecular docking and molecular dynamics simulation. *J. Biomol. Struct. Dyn.* **38**, 5230–5252. <https://doi.org/10.1080/07391102.2019.1700167> (2020).
20. Mengin-Lecreulx, D., Texier, L., Rousseau, M. & van Heijenoort, J. The murG gene of *Escherichia coli* codes for the UDP-N-acetylglucosamine: N-acetylmuramyl-(pentapeptide) pyrophosphoryl-undecaprenol N-acetylglucosamine transferase involved in the membrane steps of peptidoglycan synthesis. *J. Bacteriol.* **173**, 4625–4636. <https://doi.org/10.1128/jb.173.15.4625-4636.1991> (1991).
21. Chen, L. *et al.* Intrinsic lipid preferences and kinetic mechanism of *Escherichia coli* MurG. *Biochemistry* **41**, 6824–6833. <https://doi.org/10.1021/bi0256678> (2002).
22. Bupp, K. & van Heijenoort, J. The final step of peptidoglycan subunit assembly in *Escherichia coli* occurs in the cytoplasm. *J. Bacteriol.* **175**, 1841–1843. <https://doi.org/10.1128/jb.175.6.1841-1843.1993> (1993).
23. Ortega-Ramirez, L. A., Gutiérrez-Pacheco, M. M., Vargas-Arispuro, I., González-Aguilar, G. A., Martínez-Téllez, M. A., Ayala-Zavala, J. F. Inhibition of Glucosyltransferase Activity and Glucan Production as an Antibiofilm Mechanism of Lemongrass Essential Oil against *Escherichia coli* O157:H7. *Antibiotics* (Basel, Switzerland), <https://doi.org/10.3390/antibiotics9030102>. (2020)
24. Williams, D. A. *et al.* Metabolic inhibitors of bacterial glycan biosynthesis. *Chem. Sci.* **11**, 1761–1774. <https://doi.org/10.1039/C9SC05955E> (2020).
25. Barreteau, H. *et al.* Cytoplasmic steps of peptidoglycan biosynthesis. *FEMS Microbiol. Rev.* **32**, 168–207. <https://doi.org/10.1111/j.1574-6976.2008.00104.x> (2008).
26. Manat, G. *et al.* Deciphering the metabolism of undecaprenyl-phosphate: The bacterial cell-wall unit carrier at the membrane frontier. *Microbial. Drug Resist.* **20**, 199–214. <https://doi.org/10.1089/mdr.2014.0035> (2014).
27. Garcia-Heredia, A. Plasma membrane-cell wall feedback in bacteria. *J. Bacteriol.* **205**, e00433-e1422. <https://doi.org/10.1128/jb.00433-22> (2023).
28. Ruiz, N. Bioinformatics identification of MurJ MviN as the peptidoglycan lipid II flippase in *Escherichia coli*. *Proc. Natl. Acad. Sci.* **105**, 15553–15557. <https://doi.org/10.1073/pnas.0808352105> (2008).
29. Hu, Y. *et al.* Crystal structure of the MurG:UDP-GlcNAc complex reveals common structural principles of a superfamily of glycosyltransferases. *Proc. Natl. Acad. Sci.* **100**, 845–849. <https://doi.org/10.1073/pnas.0235749100> (2003).
30. Ha, S., Walker, D., Shi, Y. & Walker, S. The 1.9 Å crystal structure of *Escherichia coli* MurG, a membrane-associated glycosyltransferase involved in peptidoglycan biosynthesis. *Protein Sci.* **9**, 1045–1052. <https://doi.org/10.1110/ps.9.6.1045> (2000).
31. Brown, K. *et al.* Crystal structure of the pseudomonas aeruginosa MurG: UDP-GlcNAc substrate complex. *Protein Peptide Lett.* **20**, 1002–1008. <https://doi.org/10.2174/0929866511320090006> (2013).
32. Cai, X., Wang, R., Filloux, A., Waksman, G. & Meng, G. Structural and functional characterization of pseudomonas aeruginosa CupB chaperones. *PLoS One* **6**, e16583. <https://doi.org/10.1371/journal.pone.0016583> (2011).
33. Wong, K. K., Brinkman, F. S., Benz, R. S. & Hancock, R. E. Evaluation of a structural model of *Pseudomonas aeruginosa* outer membrane protein OprM, an efflux component involved in intrinsic antibiotic resistance. *J. Bacteriol.* **183**, 367–374. <https://doi.org/10.1128/jb.183.1.367-374.2001> (2001).
34. Howard, N. I. & Bugg, T. D. H. Synthesis and activity of 5'-Uridinyl dipeptide analogues mimicking the amino terminal peptide chain of nucleoside antibiotic mureidomycin A. *Biorg. Med. Chem.* **11**, 3083–3099. <https://doi.org/10.1016/S0968-08960300270-0> (2003).
35. Fang, X. *et al.* The mechanism of action of ramoplanin and enduracidin. *Mol. Biosyst.* **2**, 69–76. <https://doi.org/10.1039/B515328J> (2006).
36. Münch, D. *et al.* Structural variations of the cell wall precursor lipid II and their influence on binding and activity of the lipoglycopeptide antibiotic oritavancin. *Antimicrob. Agents Chemother.* **59**, 772–781. <https://doi.org/10.1128/aac.02663-14> (2015).
37. Dickman, R., Mitchell, S. A., Figueiredo, A. M., Hansen, D. F. & Tabor, A. B. Molecular recognition of lipid II by lantibiotics: Synthesis and conformational studies of analogues of nisin and mutacin rings A and B. *J. Org. Chem.* **84**, 11493–11512. <https://doi.org/10.1021/acs.joc.9b01253> (2019).
38. Varney, K. M. *et al.* Turning defense into offense: Defensin mimetics as novel antibiotics targeting lipid II. *PLoS Pathog.* **9**, e1003732. <https://doi.org/10.1371/journal.ppat.1003732> (2013).
39. Chen, X., Wong, C.-H. & Ma, C. Targeting the bacterial transglycosylase: Antibiotic development from a structural perspective. *ACS Infect. Dis.* **5**, 1493–1504. <https://doi.org/10.1021/acscinfecdis.9b00118> (2019).
40. Rumbo, C. *et al.* Contribution of efflux pumps, porins, and β -lactamases to multidrug resistance in clinical isolates of *Acinetobacter baumannii*. *Antimicrob. Agents Chemother.* **57**, 5247–5257. <https://doi.org/10.1128/aac.00730-13> (2013).
41. Edwards, J. R. & Betts, M. J. Carbapenems: The pinnacle of the beta-lactam antibiotics or room for improvement?. *J. Antimicrob. Chemother.* **45**, 1–4. <https://doi.org/10.1093/jac/45.1.1> (2000).
42. Radeck, J., Lautenschläger, N. & Mascher, T. The essential UPP phosphatase pair BcrC and UppP connects cell wall homeostasis during growth and sporulation with cell envelope stress response in *Bacillus subtilis*. *Front. Microbiol.* **8**, 2403. <https://doi.org/10.3389/fmicb.2017.02403> (2017).
43. Kim, S. H. *et al.* Tunicamycin-Induced ER Stress is accompanied with oxidative stress via abrogation of sulfur amino acids metabolism in the liver. *Int. J. Mol. Sci.* **19**, 4114. <https://doi.org/10.3390/ijms19124114> (2018).
44. Sarkar, P., Yarlagadda, V., Ghosh, C. & Haldar, J. A review on cell wall synthesis inhibitors with an emphasis on glycopeptide antibiotics. *MedChemComm.* **8**, 516–533. <https://doi.org/10.1039/C6MD00585C> (2017).
45. Evidente, A. Bioactive lipopeptides produced by bacteria and fungi. *Int. J. Mol. Sci.* **23**, 12342. <https://doi.org/10.3390/ijms232012342> (2022).

46. Hu, Y., Helm, J. S., Chen, L., Ye, X. Y. & Walker, S. Ramoplanin inhibits bacterial transglycosylases by binding as a dimer to lipid II. *J. Am. Chem. Soc.* **125**, 8736–8737. <https://doi.org/10.1021/ja035217i> (2003).
47. Bush, K. & Bradford, P. A. β -Lactams and β -lactamase inhibitors: An overview. *Cold Spring Harb. Perspect. Med.* <https://doi.org/10.1101/cshperspect.a025247> (2016).
48. Hu, J. *et al.* Avian pathogenic *Escherichia coli* through Pfs Affects the tran-scription of membrane proteins to resist β -lactam antibiotics. *Vet. Sci.* <https://doi.org/10.3390/vetsci9030098> (2022).
49. Drawz, S. M. & Bonomo, R. A. Three decades of beta-lactamase inhibitors. *Clin. Microbiol. Rev.* **23**, 160–201. <https://doi.org/10.1128/cmr.00037-09> (2010).
50. Lovering, A. L., de Castro, L. H., Lim, D. & Strynadka, N. C. Structural insight into the transglycosylation step of bacterial cell-wall biosynthesis. *Science*. **315**, 1402–1405. <https://doi.org/10.1126/science.1136611> (2007).
51. Nguyen R, Khanna NR, Safadi AO, *et al.* Bacitracin Topical. [Updated 2022 Nov 21]. In: StatPearls [Internet]. Treasure Island FL: StatPearls Publishing; 2023. Available from: <https://www.ncbi.nlm.nih.gov/books/NBK536993/>.
52. Zhao, H. *et al.* NPASS database update 2023: Quantitative natural product activity and species source database for biomedical research. *Nucleic Acids Res.* **51**, D621–D628. <https://doi.org/10.1093/nar/gkac1069> (2022).
53. Sorokina, M. & Steinbeck, C. Review on natural products databases: Where to find data in 2020. *J. Cheminform.* **12**, 20. <https://doi.org/10.1186/s13321-020-00424-9> (2020).
54. Zeng, X. *et al.* NPASS: natural product activity and species source database for natural product research, discovery and tool development. *Nucleic Acids Res.* **46**, D1217–d1222. <https://doi.org/10.1093/nar/gkx1026> (2018).
55. Biovia, D. S. BIOVIA discovery studio visualizer. *Softw. Version.* **20**, 779 (2017).
56. Krieger, E. & Vriend, G. YASARA View: Molecular graphics for all devices—From smartphones to workstations. *Bioinformatics* **30**, 2981–2982. <https://doi.org/10.1093/bioinformatics/btu426> (2014).
57. McGann, M. FRED pose prediction and virtual screening accuracy. *J. Chem. Inf. Model.* **51**, 578–596. <https://doi.org/10.1021/ci100436p> (2011).
58. McGann, M. FRED and HYBRID docking performance on standardized datasets. *J. Comput. Aided Mol. Des.* **26**, 897–906. <https://doi.org/10.1007/s10822-012-9584-8> (2012).
59. FRED. OpenEye Scientific Software; Santa Fe, NM, USA: 2020. 3.5.0.4. <http://www.eyesopen.com>.
60. Hawkins, P. C. D., Skillman, A. G., Warren, G. L., Ellingson, B. A. & Stahl, M. T. Conformer Generation with OMEGA: Algorithm and validation using high quality structures from the protein databank and cambridge structural database. *J. Chem. Inf. Model.* **50**, 572–584. <https://doi.org/10.1021/ci100031x> (2010).
61. Hu, Y. *et al.* Crystal structure of the MurG: UDP-GlcNAc complex reveals common structural principles of a superfamily of glycosyltransferases. *PNAS.* **100**, 845–849 (2003).
62. Spruce 1.5.3.3. OpenEye, Cadence Molecular Sciences, Santa Fe, NM. <http://www.eyesopen.com>.
63. Narykov, O. *et al.* Integration of computational docking into anti-cancer drug response prediction models. *Cancers* **161**, 50 (2023).
64. Daina, A., Michielin, O. & Zoete, V. SwissADME: a free web tool to evaluate pharmacokinetics, drug-likeness and medicinal chemistry friendliness of small molecules. *Sci. Rep.* **7**, 42717. <https://doi.org/10.1038/srep42717> (2017).
65. Yang, H. *et al.* admetSAR 2.0: Web-service for prediction and optimization of chemical ADMET properties. *Bioinformatics* **35**, 1067–1069 (2019).
66. Berendsen, H. J. C., van der Spoel, D. & van Drunen, R. GROMACS: A message-passing parallel molecular dynamics implementation. *Comput. Phys. Commun.* **91**, 43–56. <https://doi.org/10.1016/0010-46559500042-E> (1995).
67. Abraham, M. J. *et al.* GROMACS: High performance molecular simulations through multi-level parallelism from laptops to supercomputers. *SoftwareX.* **1–2**, 19–25. <https://doi.org/10.1016/j.softx.2015.06.001> (2015).
68. E. Lindahl, E., Abraham, M. J., Hess, V., van der Spoel, D. GROMACS 2020.1 Source Code; Zenodo (2020).
69. Lindorff-Larsen, K. *et al.* Systematic validation of protein force fields against experimental data. *PLoS One* **7**, e32131. <https://doi.org/10.1371/journal.pone.0032131> (2012).
70. Sousa da Silva, A. W. & Vranken, W. F. ACPYPE: AnteChamber PYthon parser interfacE. *BMC Res. Notes* **5**, 367. <https://doi.org/10.1186/1756-0500-5-367> (2012).
71. Lingenheil, M., Denschlag, R., Reichold, R. & Tavan, P. The “hot-solvent/cold-solute” problem revisited. *J. Chem. Theory Comput.* **4**, 1293–1306. <https://doi.org/10.1021/ct8000365> (2008).
72. Abraham, M. J. & Gready, J. E. Optimization of parameters for molecular dynamics simulation using smooth particle-mesh Ewald in GROMACS 4.5. *J. Comput. Chem.* **32**, 2031–2040. <https://doi.org/10.1002/jcc.21773> (2011).
73. Hess, B. P-LINCS: A parallel linear constraint solver for molecular simulation. *J. Chem. Theory Comput.* **4**, 116–122. <https://doi.org/10.1021/ct700200b> (2008).
74. Pettersen, E. F. *et al.* UCSF Chimera—a visualization system for exploratory research and analysis. *J. Comput. Chem.* **25**, 1605–1612. <https://doi.org/10.1002/jcc.20084> (2004).
75. Schrödinger, L. & DeLano, W. (2020). PyMOL, Available at: <http://www.pymol.org/pymol>.
76. Mumari, R., Kumar, R., Open Source Drug Discovery Consortium; Lynn A. g_mmpbsa—a GROMACS tool for high-throughput MM-PBSA calculations. *J. Chem. Inf. Model.* **547**, 1951–1962. <https://doi.org/10.1021/ci500020m> (2014).
77. Lipinski, C. A., Lombardo, F., Dominy, B. W. & Feeney, P. J. Experimental and computational approaches to estimate solubility and permeability in drug discovery and development settings. *Adv. Drug Delivery Rev.* **46**, 3–26. <https://doi.org/10.1016/s0169-409x000129-0> (2001).
78. Veber, D. F. *et al.* Molecular properties that influence the oral bioavailability of drug candidates. *J. Med. Chem.* **45**, 2615–2623. <https://doi.org/10.1021/jm020017n> (2002).
79. Hu, Q., Feng, M., Lai, L. & Pei, J. Prediction of drug-likeness using deep autoencoder neural networks. *Front. Genet.* <https://doi.org/10.3389/fgene.2018.00585> (2018).
80. Shin, H. K., Kang, Y.-M. & No, K. T. Predicting ADME Properties of Chemicals. In *Handbook of Computational Chemistry* (ed. Leszczynski, J.) 1–37 (Springer, 2016).
81. Arnott, J. A. & Planey, S. L. The influence of lipophilicity in drug discovery and design. *Expert Opin. Drug Discov.* **7**, 863–875. <https://doi.org/10.1517/17460441.2012.714363> (2012).
82. National Center for Biotechnology Information. PubChem Compound Summary for CID 10575622, Okaramine I. <https://pubchem.ncbi.nlm.nih.gov/compound/okaramine-I>. Accessed 20 Oct 2023.
83. National Center for Biotechnology Information. PubChem Compound Summary for CID 3008614, 2R,3R-2,3-dihydroxy-1-2,4,6-trihydroxyphenyl-3-3,4,5-trihydroxyphenylpropan-1-one. <https://pubchem.ncbi.nlm.nih.gov/compound/3008614>. Accessed 20 Oct 2023.
84. National Center for Biotechnology Information. PubChem Compound Summary for CID 5320435, Patulitrin. <https://pubchem.ncbi.nlm.nih.gov/compound/Patulitrin>. Accessed 20 Oct 2023.
85. National Center for Biotechnology Information. PubChem Compound Summary for CID 5282160, Quercimeritrin. <https://pubchem.ncbi.nlm.nih.gov/compound/Quercimeritrin>. Accessed 20 Oct 2023.
86. National Center for Biotechnology Information. PubChem Compound Summary for CID 57381071, Aflaquinolone F. <https://pubchem.ncbi.nlm.nih.gov/compound/Aflaquinolone-F>. Accessed 20 Oct 2023.

87. Ezhilarasan, V., Sharma, O. P. & Pan, A. In silico identification of potential drug targets in *Clostridium difficile* R20291: Modeling and virtual screening analysis of a candidate enzyme MurG. *Med. Chem. Res.* **22**, 2692–2705. <https://doi.org/10.1007/s00044-012-0262-0> (2013).

Acknowledgements

Amneh Shtaiwi gratefully acknowledges the financial support received from the Deanship of Graduate Studies Scientific Research, through the Pharmacy-server fund scheme, Faculty of Pharmacy, Middle East University, MEU-Jordan. Shafi Ullah Khan is the Recipient of the WINNING Normandy Program supported by the Normandy Region and this project has received funding from the European Union's Horizon 2020 research and innovation programme under the Marie Skłodowska-Curie grant agreement No 101034329. Dr. Abdelouahid Samadi thanks the United Arab Emirates University and Zayed Center for Health Sciences for the financial grants Strategic Research Program (Grant G00003680) for support. We also thank OpenEye Scientific Software for providing a free academic license to perform in silico studies.

Author contributions

A.S.: conceptualization, funding acquisition, formal analysis, investigation, methodology, resources, software, supervision, visualization, writing—original draft, methodology, writing—original draft preparation; S.U.K.: conceptualization, resources, software, validation, writing-original draft; M.K.: resources, software, investigation; M.A.: conceptualization, writing-original draft; A.S.: formal analysis, investigation, funding acquisition, conceptualization; S.C.: supervision, formal analysis, writing-review and editing. All authors gave final approval for publication and agreed to be held accountable for the work performed therein.

Competing interests

The authors declare no competing interests.

Additional information

Supplementary Information The online version contains supplementary material available at <https://doi.org/10.1038/s41598-024-57702-x>.

Correspondence and requests for materials should be addressed to A.S. or A.S.

Reprints and permissions information is available at www.nature.com/reprints.

Publisher's note Springer Nature remains neutral with regard to jurisdictional claims in published maps and institutional affiliations.



Open Access This article is licensed under a Creative Commons Attribution 4.0 International License, which permits use, sharing, adaptation, distribution and reproduction in any medium or format, as long as you give appropriate credit to the original author(s) and the source, provide a link to the Creative Commons licence, and indicate if changes were made. The images or other third party material in this article are included in the article's Creative Commons licence, unless indicated otherwise in a credit line to the material. If material is not included in the article's Creative Commons licence and your intended use is not permitted by statutory regulation or exceeds the permitted use, you will need to obtain permission directly from the copyright holder. To view a copy of this licence, visit <http://creativecommons.org/licenses/by/4.0/>.

© The Author(s) 2024